May 17, 2017

Supporting Information

Modeling Nonequilibrium Dynamics of Phase Transitions at the Nanoscale: Application to Spin-Crossover

Sang-Tae Park[†] and Renske M. van der Veen[*]

[†]*Physical Biology Center for Ultrafast Science and Technology, Arthur Amos Noyes Laboratory of Chemical Physics, California Institute of Technology, Pasadena, California 91125*

[*]*Department of Chemistry and Frederick Seitz Materials Research Laboratory, University of Illinois at Urbana-Champaign, Urbana, IL 61801, USA*

*To whom correspondence should be addressed: renske@illinois.edu

S.I Differential Scanning Calorimetry

Fig. S1 shows the differential scanning calorimetry (DSC) results on a polycrystalline Fe(pz)Pt(CN)$_4$ sample. Two well-defined peaks in the heat capacity at 297 K (heating) and 277 K (cooling) are observed. The change in enthalpy is obtained by integrating the areas underneath the phase transition peaks above the base line, giving $\Delta H = 21$ kJ/mol (heating) and $\Delta H = 22$ kJ/mol (cooling). Since we do not consider hysteresis in the present work, we take the average of the two ΔH values, $\Delta H_{av} = 21.5$ kJ/mol, and use it in the heat diffusion simulations. Note that the absolute heat capacity values for the LS state and HS state can not be obtained from these results due to insufficient calibration of the DSC apparatus. Measured changes in the heat capacity, however, are expected to be accurate to within a few %.

We adopt a constant heat capacity of $C_p = 250$ J/K/mol for both LS and HS and ignore any temperature dependence for simplicity.[1,2]

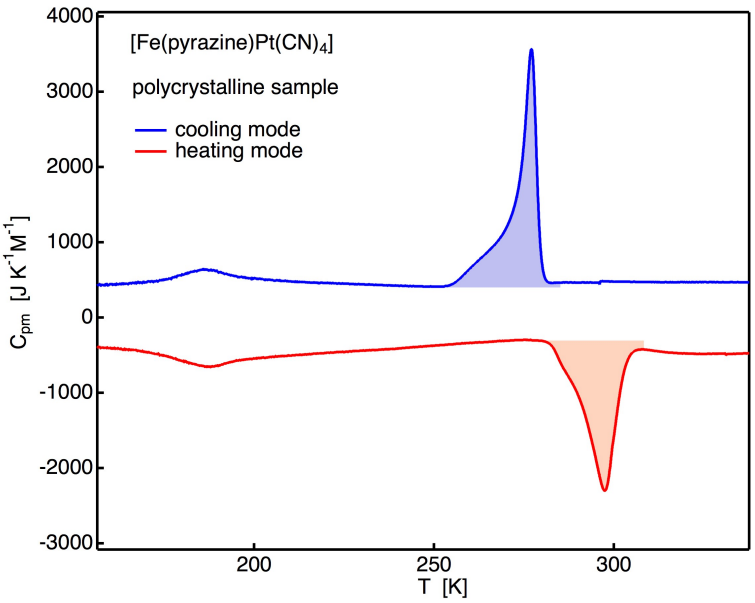

Figure S1: Differential scanning calorimetry of a polycrystalline Fe(pyrazine)Pt(CN)$_4$ sample. The colored shading represents the areas that where integrated to determine the change in enthalpy.

S.II Time-resolved optical experiments on nanoparticle ensembles

S.II.1 Relaxation profiles

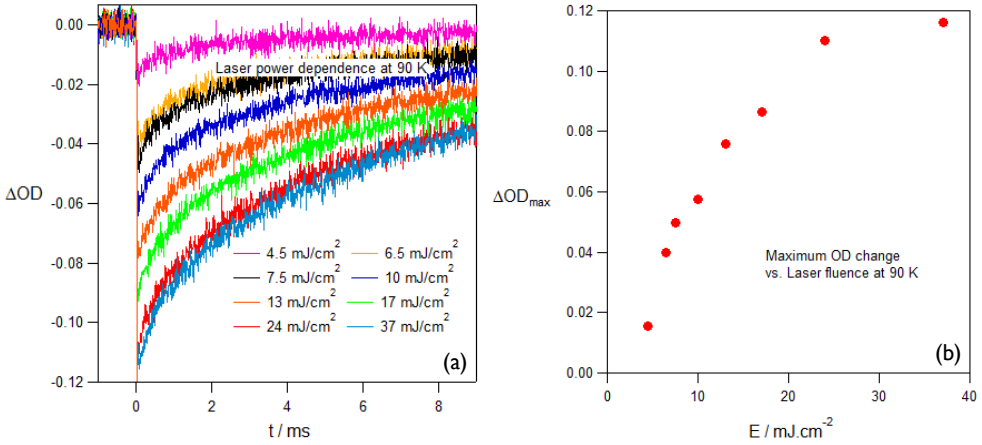

Figure S2: (a) Pump-probe time profiles recorded at 90 K on an ensemble of nanoparticles with a pulsed 532 nm laser at 20 Hz and for different laser fluences. The evolution of the absorbance following the laser pulse has been probed at 570 nm. (b) Maximum change in optical density (OD) as a function of laser fluence. An OD change of 0.11 corresponds to an excitation yield of 20% (*i.e.* 20% of the spin-crossover center are converted from the LS state to the HS state.

S.II.2 Rate constants

Solving the coupled differential equations for temperature and fraction, eqns. (3) and (4) in the main text, requires the prior knowledge of the rate constants of the spin crossover reaction. The reverse reaction (relaxation of HS state to LS state) rate constants at various temperatures below the phase transition were measured via optical spectroscopy (see S.II.1). The results are plotted in Fig. S3, and fitted to Eyring-Polanyi equation, eqn. (6) in the main text. We obtain $\Delta H_h^{\ddagger} = 11 \pm 2$ kJmol^{-1} and $\Delta S_h^{\ddagger} = -79 \pm 10$ J K^{-1}mol^{-1}, which we assume are constants over the entire temperature range in our simulation. The equilibration constant, K, was measured via electron diffraction (see Fig. 2 in the main text), and fitted to eqn. (8) in the main text, assuming $\Delta H = 21$ kJ mol^{-1}, we obtain $\Delta S = 87 \pm 17$ J K^{-1} mol^{-1}. Then, we obtain $\Delta H_l^{\ddagger} = 32 \pm 2$ kJ mol^{-1} and $\Delta S_l^{\ddagger} = 8 + / - 19$ J K^{-1} mol^{-1}, with which we calculate the forward reaction time constant using the Eyring-Polanyi equation.

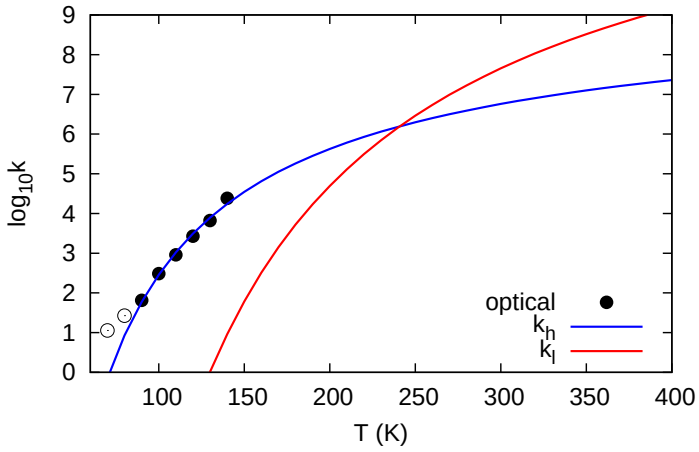

Figure S3: Temperature dependence of the forward, k_l, and reverse, k_h, reaction rate constants for the LS-HS SCO phase transition in Fe(pyrazine)Pt(CN)$_4$. The circles denote the data points from the optical time-resolved HS→LS relaxation measurements. The blue curve represents the fit of the Eyring-Polanyi equation (eqn. (6) in the main text) to the data in the temperature range 90-150 K (black circles). The red curve is then obtained using the expressions for the equilibrium constant (eqn. (7) and (8) in the main text).

S.III Thermal parameters of the graphite substrate

Fig. S4 shows the temperature dependences of the thermal properties of the graphite substrate used in the simulations. The temperature-dependent thermal conductivity (Fig. S4a) was taken from Refs.[3] and[4] and then modified using eqn. (11) with $k_c = 62$ W/K/m in order to obtain best agreement to our experimental data (Fig. 3 in the main text).

The temperature-dependent heat capacity of pyrolytic graphite (Fig. S4b) was taken from Ref.[4] without modification.

The change of lattice parameter of the graphite substrate was modeled as a mixture of graphite[5] (92%) and graphene[6] (8%), the latter representing the flakiness of the CVD graphite film. Graphene exhibits a higher negative thermal expansion over an extended temperature range,[6] the admixture of which results in a better agreement with our data. The resulting modified thermal expansion properties of graphite are plotted in Fig. S4c.

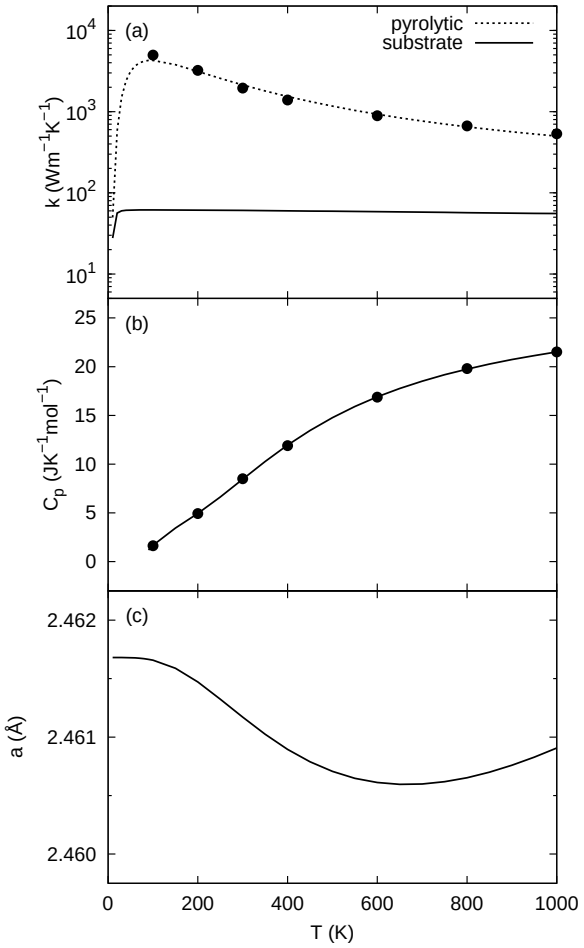

Figure S4: Temperature dependence of the thermal properties of graphite used in the simulations (solid lines): (a) thermal conductivity, (b) heat capacity, and (c) lattice parameter. Black circles are taken from Ref. [4]

References

[1] V. Niel, J. Martinez-Agudo, M. Munoz, A. Gaspar and J. Real, *Inorg. Chem*, 2001, **40**, 3838.

[2] M. A. Halcrow, *Spin-Crossover Materials*, John Wiley & Sons, 2013.

[3] C. Uher, in *SpringerMaterials-The Landolt-Börnstein Database*, ed. O. Madelung and G. K. White, Springer-Verlag, Berlin, 1991.

[4] F. P. Incropera, *Fundamentals of heat and mass transfer*, John Wiley, Hoboken, NJ, 6th edn., 2007.

[5] W. C. Morgan, *Carbon*, 1972, **10**, 73–79.

[6] N. Mounet and N. Marzari, *Phys. Rev. B*, 2005, **71**, 205214.